Transport and Communications Science Journal

NONLINEAR BUCKLING AND POSTBUCKLING ANALYSIS OF FG-GRMMC CYLINDRICAL PANELS WITH OBLIQUE AND ORTHOGONAL STIFFENERS IN THERMAL ENVIRONMENT

Dang Thuy Dong[1,2], Dao Huy Bich[3], Pham Nhu Nam[3,4], Pham Thanh Hieu[4] Nguyen Thi Phuong[1,2*]

[1]Institute for Advanced Study in Technology, Ton Duc Thang University, No. 19 Nguyen Huu Tho Street, Ho Chi Minh City, Vietnam
[2]Faculty of Civil Engineering, Ton Duc Thang University, No. 19 Nguyen Huu Tho Street, Ho Chi Minh City, Vietnam
[3]Faculty of Mathematics, Mechanics and Informatics, VNU University of Science, No. 334 Nguyen Trai Street, Hanoi, Vietnam
[4]University of Transport Technology, No. 54 Trieu Khuc Street, Hanoi, Vietnam

ARTICLE INFO

TYPE: Research Article
Received: 12/10/2025
Revised: 24/11/2025
Accepted: 16/12/2025
Published online: 15/01/2026
https://doi.org/10.47869/tcsj.77.1.6

* *Corresponding author*
Email: nguyenthiphuong@tdtu.edu.vn; Tel: +84916074589

Abstract. Advanced composite materials, with their superior strength-to-weight ratio, durability, and thermal resistance, are increasingly applied in civil engineering for withstanding harsh mechanical and environmental loads. This paper presents a nonlinear stability analysis of cylindrical panels made from a new type of composite material, namely, functionally graded graphene-reinforced metal matrix composite (FG-GRMMC). The panels are stiffened by oblique or orthogonal FG-GRMMC stiffeners. The fundamental formulation is developed using higher-order shear deformation theory (HSDT), incorporating von Kármán geometric nonlinearity. The effects of stiffeners are modeled using an enhanced smeared stiffener technique for both mechanical and thermal effects through coordinate transformation. The governing equations are derived and solved using the Ritz energy method. Different graphene distribution patterns and stiffener orientations are systematically investigated to evaluate their effects on critical buckling and postbuckling responses. The results highlight the significant improvements in structural stability achieved through the use of oblique stiffeners and optimized material, particularly under thermal loading conditions.

Keywords: functionally graded graphene-reinforced metal matrix composite, cylindrical panels, oblique stiffeners, nonlinear buckling, energy method, thermal environment.

1. INTRODUCTION

Functionally graded materials (FGMs) are an advanced class of composite materials. Their material properties vary continuously, allowing for tailored thermomechanical properties throughout the structure. Among FGMs, functionally graded carbon nanotube-reinforced composites (FG-CNTRCs) and graphene-reinforced composites (FG-GRCs) have been widely studied due to their high stiffness and excellent thermal conductivity. Recently, functionally graded graphene-reinforced metal matrix composites (FG-GRMMCs) have emerged as a promising material. They combine the reinforcement efficiency of graphene platelets with the high strength and ductility of metal matrix. The result is enhanced structural stability in thermal environments.

The nonlinear buckling and postbuckling behavior of FGM cylindrical panels in thermal environments has been extensively studied using advanced analytical techniques. Shen and Wang [1,2] employed higher-order shear deformation theory (HSDT) and von Kármán geometric nonlinearity to investigate thermomechanical responses of FGM panels on elastic foundations. Norouzi and Alibeigloo [3] used three-dimensional elasticity theory and state-space approaches to capture viscoelastic effects, while Zhang et al. [4] and Mirzaei and Seyedi [5] analyzed thermally induced dynamic responses using Chebyshev-Ritz and Newmark integration methods. Bich et al. [6] analyzed the nonlinear dynamic buckling behavior of eccentrically stiffened FGM cylindrical panels using von Kármán–Donnell kinematics and the smeared stiffener approach, highlighting the role of imperfections and stiffener configuration. Furthermore, Dong et al. [7] developed an analytical framework for thermomechanical buckling of obliquely stiffened sandwich FGM plates on nonlinear elastic foundations, incorporating HSDT, von Kármán nonlinearity, and an extended Lekhnitskii smeared stiffener model with coordinate transformation. The governing equations of the problem were solved using the Galerkin method.

FG-CNTRC structures have been widely explored for their nonlinear mechanical responses under thermal and mechanical loading. Babaei [8] and Keleshteri et al. [9] investigated snap-buckling and snap-through phenomena in FG-CNTRC panels and plates using HSDT and perturbation or differential quadrature methods, under the influences of CNT distribution, boundary constraints, and foundation effects. Shen and Xiang [10,11] presented thermal postbuckling analyses of FG-CNTRC cylindrical panels resting on elastic foundations, employing micromechanical modeling, HSDT, and singular perturbation techniques. Nonlinear vibration and buckling of imperfect FG-CNTRC panels were addressed by Foroutan et al. [12] using Galerkin and Runge-Kutta methods, with attention to the distribution law of CNTs and an initial imperfection. Minh et al. [13] extended the smeared stiffener technique for oblique FG-CNTRC stiffeners to investigate the nonlinear stability behavior of stiffened plates using analytical solutions and Reddy's HSDT. Duc et al. [14] examined nonlinear dynamics of CNT-reinforced panels with complex curvature, piezoelectric layers, and CNT-reinforced stiffeners, using an advanced homogenization technique and dynamic buckling criteria to obtain complex structural responses.

FG-GRC and FG-GRMMC have attracted much attention due to their exceptional mechanical properties and the ability to tune the stiffness by continuously varying the Graphene content along the thickness. Shen et al. [15–17] investigated the thermal postbuckling behavior of FG-GRC and FG-GRMMC cylindrical panels using HSDT and von Kármán nonlinearity, taking into account the effects of temperature-dependent material

properties, elastic foundations, and auxetic in-plane Poisson's ratio based on the singular perturbation technique. Phuong et al. [18] developed the smeared stiffener technique for stiffened FG-GRC laminated plates with anisotropic stiffeners, employing the Galerkin method to analyze the nonlinear postbuckling response problem.

Although numerous works have addressed the nonlinear stability of stiffened FGM structures, to the best of the authors' knowledge, no studies have investigated FG-GRMMC cylindrical panels reinforced with oblique stiffeners. In addition, most previous studies have focused on isotropic orthogonal stiffeners, without comprehensive studies on the benefits of oblique FG-GRMMC stiffeners. This study develops an analytical model based on HSDT and von Kármán nonlinearity, incorporating a transformed smeared stiffener technique and Ritz method, to analyze the buckling and postbuckling behavior of FG-GRMMC cylindrical panels under mechanical loads in thermal environments. The influences of stiffener orientation, graphene distribution laws, geometric and material parameters are investigated in detail.

2. THEORETICAL MODELLING AND RITZ-BASED SOLUTION

This study considers stiffened FG-GRMMC cylindrical panels, subjected to external pressure and axial compression. The geometric parameters include the thickness h, straight edge length a, and curved edge length b. Two types of stiffener arrangements are considered, including orthogonal and oblique stiffener systems, as illustrated in Fig. 1. Due to the shallowness of the cylindrical panel, a Cartesian coordinate system (x,y,z) is adopted, with the origin located at the mid-surface of the panel. The panels are subjected to a thermal environment with a uniform temperature change of ΔT.

Graphene sheets (GRSs) are reinforced in a copper (Cu) matrix, with volume fractions varying from 0.05 to 0.13, and are distributed separately across ten layers along the panel thickness. Five graphene distribution types are considered in this paper. FG-V and FG-A types are characterized by asymmetric volume fraction distribution of GRSs along the thickness; FG-X and FG-O types, following symmetric GRSs distribution types; and the uniform distribution of GRSs case corresponding to a constant volume fraction across all layers. To ensure material continuity in the panel and stiffeners, five material models of the stiffened panel are considered in this study, including UD/UD, X/X, O/O, V/Λ, and Λ/V, depicted in Figure 1. In addition, the orientation of graphene sheets in the polymer matrix is also varied, with three specimens of the FG-GRC panel/ stiffener being unidirectional $(0)_{10T}$, cross-ply $(0/90)_{5T}$, and symmetric cross-ply $(0/90/0/90/0)_S$. Thermoplastic properties for the GRMMC are adopted from Fan et al. [19].

The panel is assumed to be moderately thick and geometrically imperfect strain–displacement relations are established based on HSDT, taking into account the von Kármán nonlinear strain terms and initial geometric imperfections w^* as

$$\begin{Bmatrix}\varepsilon_x\\ \varepsilon_y\\ \gamma_{xy}\end{Bmatrix}=\begin{Bmatrix}\hat{\varepsilon}_x^0\\ \hat{\varepsilon}_y^0\\ \hat{\gamma}_{xy}^0\end{Bmatrix}+z\begin{Bmatrix}\hat{\varepsilon}_x^1\\ \hat{\varepsilon}_y^1\\ \hat{\gamma}_{xy}^1\end{Bmatrix}+z^3\begin{Bmatrix}\hat{\varepsilon}_x^3\\ \hat{\varepsilon}_y^3\\ \hat{\gamma}_{xy}^3\end{Bmatrix},\qquad \begin{Bmatrix}\gamma_{xz}\\ \gamma_{yz}\end{Bmatrix}=\begin{Bmatrix}\hat{\gamma}_{xz}^0\\ \hat{\gamma}_{yz}^0\end{Bmatrix}+z^2\begin{Bmatrix}\hat{\gamma}_{xz}^2\\ \hat{\gamma}_{yz}^2\end{Bmatrix}, \quad (1)$$

where

$$\begin{Bmatrix}\hat{\varepsilon}_x^0\\ \hat{\varepsilon}_y^0\\ \hat{\gamma}_{xy}^0\end{Bmatrix}=\begin{Bmatrix}u_{,x}+w_{,x}^2/2+w_{,x}w_{,x}^*\\ v_{,y}+w_{,y}^2/2+w_{,y}w_{,y}^*-w/R\\ v_{,x}+u_{,y}+w_{,x}w_{,y}+w_{,y}w_{,x}^*+w_{,x}w_{,y}^*\end{Bmatrix},\begin{Bmatrix}\hat{\varepsilon}_x^1\\ \hat{\varepsilon}_y^1\\ \hat{\gamma}_{xy}^1\end{Bmatrix}=\begin{Bmatrix}\phi_{x,x}\\ \phi_{y,y}\\ \phi_{y,x}+\phi_{x,y}\end{Bmatrix},\lambda=\frac{4}{3h^2},$$
$$\begin{Bmatrix}\hat{\varepsilon}_x^3\\ \hat{\varepsilon}_y^3\\ \hat{\gamma}_{xy}^3\end{Bmatrix}=-\lambda\begin{Bmatrix}w_{,xx}+\phi_{x,x}\\ w_{,yy}+\phi_{y,y}\\ \phi_{y,x}+2w_{,xy}+\phi_{x,y}\end{Bmatrix},\begin{Bmatrix}\hat{\gamma}_{xz}^0\\ \hat{\gamma}_{yz}^0\end{Bmatrix}=\begin{Bmatrix}w_{,x}+\phi_x\\ w_{,y}+\phi_y\end{Bmatrix},\begin{Bmatrix}\hat{\gamma}_{xz}^2\\ \hat{\gamma}_{yz}^2\end{Bmatrix}=-3\lambda\begin{Bmatrix}w_{,x}+\phi_x\\ w_{,y}+\phi_y\end{Bmatrix}. \quad (2)$$

Hooke's law is applied to both the panel and stiffeners, incorporating thermal strain effects, expressed as

$$\begin{bmatrix}\sigma_{xx}\\ \sigma_{yy}\\ \sigma_{xy}\end{bmatrix}_{(k)}=\begin{bmatrix}Q_{11}&Q_{12}&0\\ Q_{12}&Q_{22}&0\\ 0&0&Q_{66}\end{bmatrix}_{(k)}\begin{bmatrix}\varepsilon_{xx}-\alpha_{11}\Delta T\\ \varepsilon_{yy}-\alpha_{22}\Delta T\\ \gamma_{xy}\end{bmatrix}_{(k)},$$
$$\sigma_{xy}=Q_{66(k)}\gamma_{xy},\quad \sigma_{xz}=Q_{44(k)}\gamma_{xz},\quad \sigma_{yz}=Q_{55(k)}\gamma_{yz}, \quad (3)$$

where $Q_{ij(k)}$ denotes the reduced stiffness of the k-th GRMMC layer.

The in-plane forces and bending moments of the FG-GRMMC panel reinforced by either orthogonal or oblique stiffeners are formulated by combining an improved smeared stiffener technique (based on Lekhnitskii smeared stiffener technique with a coordinate transformation method) to include both mechanical and thermal contributions as follows

$$\begin{Bmatrix}N_x\\ N_y\\ N_{xy}\\ M_x\\ M_y\\ M_{xy}\\ T_x\\ T_y\\ T_{xy}\end{Bmatrix}=\begin{bmatrix}D_{11}&D_{12}&0&A_{11}&A_{12}&0&F_{11}&F_{12}&0\\ D_{12}&D_{22}&0&A_{12}&A_{22}&0&F_{12}&F_{22}&0\\ 0&0&D_{66}&0&0&A_{66}&0&0&F_{66}\\ A_{11}&A_{12}&0&L_{11}&L_{12}&0&H_{11}&H_{12}&0\\ A_{12}&A_{22}&0&L_{12}&L_{22}&0&H_{12}&H_{22}&0\\ 0&0&A_{66}&0&0&L_{66}&0&0&H_{66}\\ F_{11}&F_{12}&0&H_{11}&H_{12}&0&G_{11}&G_{12}&0\\ F_{12}&F_{22}&0&H_{12}&H_{22}&0&G_{12}&G_{22}&0\\ 0&0&F_{66}&0&0&H_{66}&0&0&G_{66}\end{bmatrix}\begin{bmatrix}\hat{\varepsilon}_x^0\\ \hat{\varepsilon}_y^0\\ \hat{\gamma}_{xy}^0\\ \hat{\varepsilon}_x^1\\ \hat{\varepsilon}_y^1\\ \hat{\gamma}_{xy}^1\\ \hat{\varepsilon}_x^3\\ \hat{\varepsilon}_y^3\\ \hat{\gamma}_{xy}^3\end{bmatrix}-\begin{bmatrix}\Phi_{1x}\\ \Phi_{1y}\\ 0\\ \Phi_{2x}\\ \Phi_{2y}\\ 0\\ \Phi_{4x}\\ \Phi_{4y}\\ 0\end{bmatrix}\Delta T, \quad (4)$$

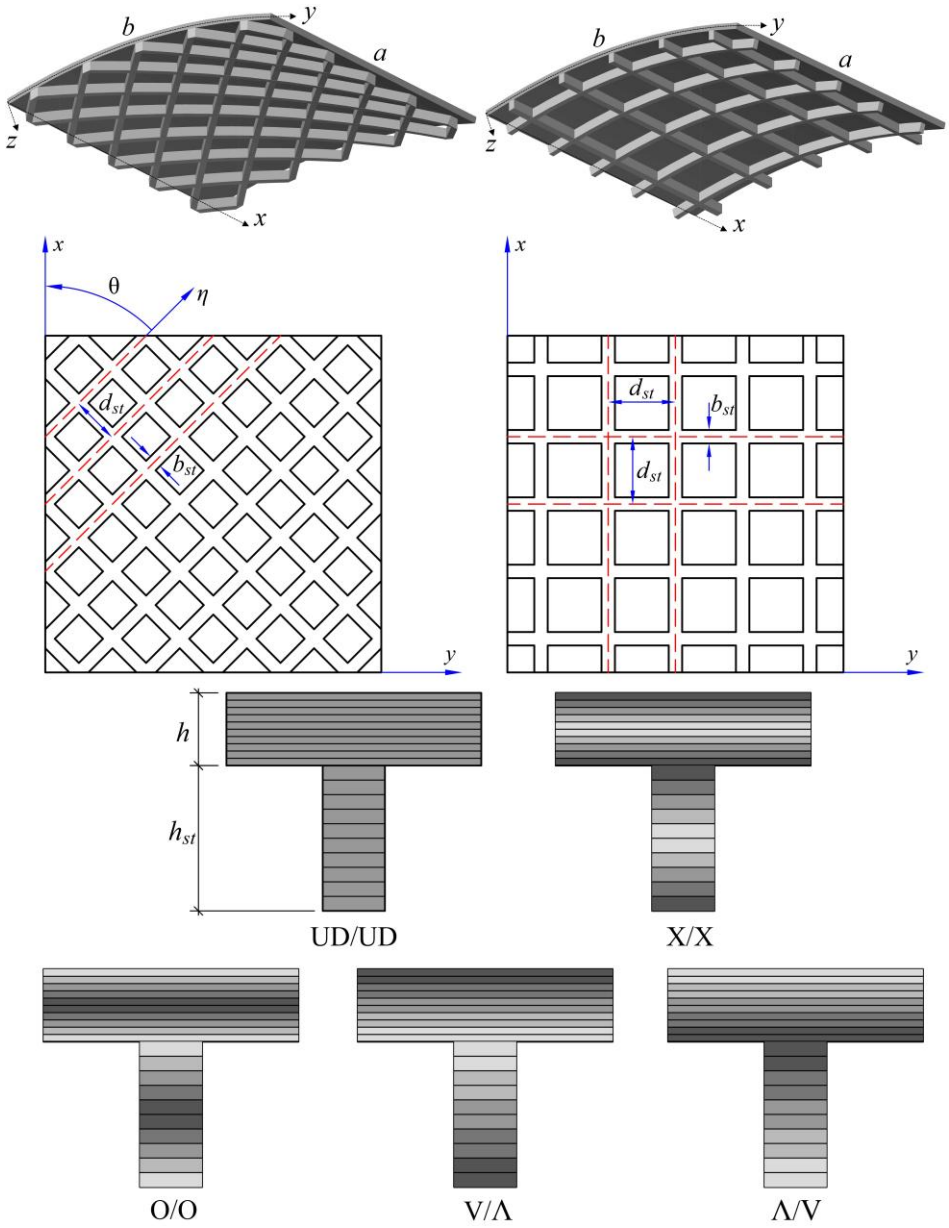

Fig. 1. Configuration, coordinate system, and stiffener design of FG-GRMMC cylindrical panels.

The expressions for shear forces and higher-order shear forces are given by

$$\begin{bmatrix} Q_x \\ Q_y \\ S_x \\ S_y \end{bmatrix} = \begin{bmatrix} B_{44} & 0 & E_{44} & 0 \\ 0 & B_{55} & 0 & E_{55} \\ E_{44} & 0 & C_{44} & 0 \\ 0 & E_{55} & 0 & C_{55} \end{bmatrix} \begin{bmatrix} \hat{\gamma}^0_{xz} \\ \hat{\gamma}^0_{yz} \\ \hat{\gamma}^2_{xz} \\ \hat{\gamma}^2_{yz} \end{bmatrix}, \tag{5}$$

where

$$D_{11} = D_{11sh} + \mu_1 \frac{b_{st}}{d_{st}} D^{st}_{11} + 2\mu_2 \frac{b_{st}}{d_{st}} D^{st}_{11} \cos^4\theta, D_{12} = D_{12sh} + 2\mu_2 \frac{b_{st}}{d_{st}} D^{st}_{11} \cos^2\theta \sin^2\theta,$$

$$D_{22} = D_{22sh} + \mu_1 \frac{b_{st}}{d_{st}} D_{22}^{st} + 2\mu_2 \frac{b_{st}}{d_{st}} D_{11}^{st} \sin^4\theta, D_{66} = D_{66sh} + 2\mu_2 \frac{b_{st}}{d_{st}} D_{11}^{st} \cos^2\theta \sin^2\theta,$$

$$A_{11} = A_{11sh} + \mu_1 \frac{b_{st}}{d_{st}} A_{11}^{st} + 2\mu_2 \frac{b_{st}}{d_{st}} A_{11}^{st} \cos^4\theta, A_{12} = A_{12sh} + 2\mu_2 \frac{b_{st}}{d_{st}} A_{11}^{st} \cos^2\theta \sin^2\theta,$$

$$A_{22} = A_{22sh} + \mu_1 \frac{b_{st}}{d_{st}} A_{22}^{st} + 2\mu_2 \frac{b_{st}}{d_{st}} A_{11}^{st} \sin^4\theta, A_{66} = A_{66sh} + 2\mu_2 \frac{b_{st}}{d_{st}} A_{11}^{st} \cos^2\theta \sin^2\theta,$$

$$F_{11} = F_{11sh} + \mu_1 \frac{b_{st}}{d_{st}} F_{11}^{st} + 2\mu_2 \frac{b_{st}}{d_{st}} F_{11}^{st} \cos^4\theta,\ F_{12} = F_{12sh} + 2\mu_2 \frac{b_{st}}{d_{st}} F_{11}^{st} \cos^2\theta \sin^2\theta,$$

$$F_{22} = F_{22sh} + \mu_1 \frac{b_{st}}{d_{st}} F_{22}^{st} + 2\mu_2 \frac{b_{st}}{d_{st}} F_{11}^{st} \sin^4\theta,\ F_{66} = F_{66sh} + 2\mu_2 \frac{b_{st}}{d_{st}} F_{11}^{st} \cos^2\theta \sin^2\theta,$$

$$L_{11} = L_{11sh} + \mu_1 \frac{b_{st}}{d_{st}} L_{11}^{st} + 2\mu_2 \frac{b_{st}}{d_{st}} L_{11}^{st} \cos^4\theta,\ L_{12} = L_{12sh} + 2\mu_2 \frac{b_{st}}{d_{st}} L_{11}^{st} \cos^2\theta \sin^2\theta,$$

$$L_{22} = L_{22sh} + \mu_1 \frac{b_{st}}{d_{st}} L_{22}^{st} + 2\mu_2 \frac{b_{st}}{d_{st}} L_{11}^{st} \sin^4\theta,\ L_{66} = L_{66sh} + 2\mu_2 \frac{b_{st}}{d_{st}} L_{11}^{st} \cos^2\theta \sin^2\theta,$$

$$H_{11} = H_{11sh} + \mu_1 \frac{b_{st}}{d_{st}} H_{11}^{st} + 2\mu_2 \frac{b_{st}}{d_{st}} H_{11}^{st} \cos^4\theta, H_{12} = H_{12sh} + 2\mu_2 \frac{b_{st}}{d_{st}} H_{11}^{st} \cos^2\theta \sin^2\theta,$$

$$H_{22} = H_{22sh} + \mu_1 \frac{b_{st}}{d_{st}} H_{22}^{st} + 2\mu_2 \frac{b_{st}}{d_{st}} H_{11}^{st} \sin^4\theta, H_{66} = H_{66sh} + 2\mu_2 \frac{b_{st}}{d_{st}} H_{11}^{st} \cos^2\theta \sin^2\theta,$$

$$G_{11} = G_{11sh} + \mu_1 \frac{b_{st}}{d_{st}} G_{11}^{st} + 2\mu_2 \frac{b_{st}}{d_{st}} G_{11}^{st} \cos^4\theta,\ G_{12} = G_{12sh} + 2\mu_2 \frac{b_{st}}{d_{st}} G_{11}^{st} \cos^2\theta \sin^2\theta,$$

$$G_{22} = G_{22sh} + \mu_1 \frac{b_{st}}{d_{st}} G_{22}^{st} + 2\mu_2 \frac{b_{st}}{d_{st}} G_{11}^{st} \sin^4\theta,\ G_{66} = G_{66sh} + 2\mu_2 \frac{b_{st}}{d_{st}} G_{11}^{st} \cos^2\theta \sin^2\theta,$$

$$B_{44} = B_{44sh} + \mu_1 \frac{b_{st}}{d_{st}} B_{44}^{st} + 2\mu_2 \frac{b_{st}}{d_{st}} B_{44}^{st} \sin^2\theta, E_{44} = E_{44sh} + \mu_1 \frac{b_{st}}{d_{st}} E_{44}^{st} + 2\mu_2 \frac{b_{st}}{d_{st}} E_{44}^{st} \sin^2\theta,$$

$$C_{44} = C_{44sh} + \mu_1 \frac{b_{st}}{d_{st}} C_{44}^{st} + 2\mu_2 \frac{b_{st}}{d_{st}} C_{44}^{st} \sin^2\theta, B_{55} = B_{55sh} + \mu_1 \frac{b_{st}}{d_{st}} B_{55}^{st} + 2\mu_2 \frac{b_{st}}{d_{st}} B_{44}^{st} \cos^2\theta,$$

$$E_{55} = E_{55sh} + \mu_1 \frac{b_{st}}{d_{st}} E_{55}^{st} + 2\mu_2 \frac{b_{st}}{d_{st}} E_{44}^{st} \cos^2\theta, C_{55} = C_{55sh} + \mu_1 \frac{b_{st}}{d_{st}} C_{55}^{st} + 2\mu_2 \frac{b_{st}}{d_{st}} C_{44}^{st} \cos^2\theta,$$

$$\Phi_{1x} = \Phi_{1xsh} + \mu_1 \frac{b_{st}}{d_{st}} \Phi_{1x}^{st} + 2\mu_2 \frac{b_{st}}{d_{st}} \Phi_{1x}^{st} \left(\sin^6\theta + \sin^2\theta \cos^2\theta\right),$$

$$\Phi_{2x} = \Phi_{2xsh} + \mu_1 \frac{b_{st}}{d_{st}} \Phi_{2x}^{st} + 2\mu_2 \frac{b_{st}}{d_{st}} \Phi_{2x}^{st} \left(\sin^6\theta + \sin^2\theta \cos^2\theta\right),$$

$$\Phi_{4x} = \Phi_{4xsh} + \mu_1 \frac{b_{st}}{d_{st}} \Phi_{4x}^{st} + 2\mu_2 \frac{b_{st}}{d_{st}} \Phi_{4x}^{st} \left(\sin^6\theta + \sin^2\theta \cos^2\theta\right),$$

$$\Phi_{1y} = \Phi_{1ysh} + \mu_1 \frac{b_{st}}{d_{st}} \Phi_{1y}^{st} + 2\mu_2 \frac{b_{st}}{d_{st}} \Phi_{1x}^{st} \left(\sin^6\theta + \sin^2\theta \cos^2\theta\right),$$

$$\Phi_{2y} = \Phi_{2ysh} + \mu_1 \frac{b_{st}}{d_{st}} \Phi_{2y}^{st} + 2\mu_2 \frac{b_{st}}{d_{st}} \Phi_{2x}^{st} \left(\sin^6\theta + \sin^2\theta \cos^2\theta \right),$$

$$\Phi_{4y} = \Phi_{4ysh} + \mu_1 \frac{b_{st}}{d_{st}} \Phi_{4y}^{st} + 2\mu_2 \frac{b_{st}}{d_{st}} \Phi_{4x}^{st} \left(\sin^6\theta + \sin^2\theta \cos^2\theta \right),$$

with the parameters μ_1 and μ_2 denote the stiffener parameters: $\mu_1 = 1$ and $\mu_2 = 0$ corresponds to orthogonal stiffeners, $\mu_1 = 0$ and $\mu_2 = 1$ corresponds to oblique stiffeners, and $\mu_1 = 0$ and $\mu_2 = 0$ represents an unstiffened panel, and

$$\left(D_{ijsh}, A_{ijsh}, L_{ijsh}, F_{ijsh}, H_{ijsh}, G_{ijsh} \right)_{(k)} = \sum_{k=1}^{10} \int_{\Xi(k)} Q_{ij(k)} \left(1,\ z, z^2, z^3, z^4, z^6 \right) dz, \quad (i, j = 1,2,6),$$

$$\left(B_{ijsh}, E_{ijsh}, C_{ijsh} \right)_{(k)} = \sum_{k=1}^{10} \int_{\Xi(k)} Q_{ij(k)} \left(1, z^2, z^4 \right) dz, \quad (i, j = 4,5),$$

$$\left(\Phi_{1x}, \Phi_{2x}, \Phi_{4x} \right)_{(k)} = \sum_{k=1}^{10} \int_{\Xi(k)} \left[Q_{11(k)} \alpha_{11(k)} + Q_{12(k)} \alpha_{22(k)} \right] \left(1, z^2, z^3 \right) dz,$$

$$\left(\Phi_{1y}, \Phi_{2y}, \Phi_{4y} \right)_{(k)} = \sum_{k=1}^{10} \int_{\Xi(k)} \left[Q_{12(k)} \alpha_{11(k)} + Q_{22(k)} \alpha_{22(k)} \right] \left(1, z^2, z^3 \right) dz,$$

where $\Xi(k)$ are the domains of integration in the thickness direction of the GRMMC layers, respectively, and

$$\begin{bmatrix} D_{st}^i & A_{st}^i & F_{st}^i \\ A_{st}^i & L_{st}^i & H_{st}^i \\ F_{st}^i & H_{st}^i & G_{st}^i \end{bmatrix} = \begin{bmatrix} \bar{D}_i & \bar{A}_i & \bar{F}_i \\ \bar{A}_i & \bar{L}_i & \bar{H}_i \\ \bar{F}_i & \bar{H}_i & \bar{G}_i \end{bmatrix} - \begin{bmatrix} \bar{D}_{12} & 0 & \bar{A}_{12} & 0 & \bar{F}_{12} & 0 \\ \bar{A}_{12} & 0 & \bar{L}_{12} & 0 & \bar{H}_{12} & 0 \\ \bar{F}_{12} & 0 & \bar{H}_{12} & 0 & \bar{G}_{12} & 0 \end{bmatrix}$$

$$\times \begin{bmatrix} \bar{D}_i & 0 & \bar{A}_i & 0 & \bar{F}_i & 0 \\ 0 & \bar{D}_{66} & 0 & \bar{A}_{66} & 0 & \bar{F}_{66} \\ \bar{A}_i & 0 & \bar{L}_i & 0 & \bar{H}_i & 0 \\ 0 & \bar{A}_{66} & 0 & \bar{L}_{66} & 0 & \bar{H}_{66} \\ \bar{F}_i & 0 & \bar{H}_i & 0 & \bar{F}_{66} & 0 \\ 0 & \bar{G}_{22} & 0 & \bar{H}_{66} & 0 & \bar{G}_{66} \end{bmatrix}^{-1} \begin{bmatrix} \bar{D}_{12} & \bar{A}_{12} & \bar{F}_{12} \\ 0 & 0 & 0 \\ \bar{A}_{12} & \bar{L}_{12} & \bar{H}_{12} \\ 0 & 0 & 0 \\ \bar{F}_{12} & \bar{H}_{12} & \bar{G}_{12} \\ 0 & 0 & 0 \end{bmatrix}, \quad (i = 11, 22)$$

$$\left(\bar{D}_{ij}, \bar{A}_{ijsh}, \bar{L}_{ijsh}, \bar{F}_{ijsh}, \bar{H}_{ijsh}, \bar{G}_{ijsh} \right)_{(k)} = \sum_{k=1}^{10} \int_{\Delta(k)} Q_{ij(k)} \left(1,\ z, z^2, z^3, z^4, z^6 \right) dz, \quad (i, j = 1,2,6),$$

$$\left(B_{ij}^{st}, E_{ij}^{st}, C_{ij}^{st} \right)_{(k)} = \sum_{k=1}^{10} \int_{\Delta(k)} Q_{ij(k)} \left(1, z^2, z^4 \right) dz, \quad (i, j = 4,5),$$

$$\left(\Phi_{1x}^{st},\Phi_{2x}^{st},\Phi_{4x}^{st}\right)_{(k)}=\sum_{k=1}^{10}\int_{\Delta(k)}\left[Q_{11(k)}\alpha_{11(k)}+Q_{12(k)}\alpha_{22(k)}\right]\left(1,z^2,z^3\right)dz,$$

$$\left(\Phi_{1y}^{st},\Phi_{2y}^{st},\Phi_{4y}^{st}\right)_{(k)}=\sum_{k=1}^{10}\int_{\Delta(k)}\left[Q_{12(k)}\alpha_{11(k)}+Q_{22(k)}\alpha_{22(k)}\right]\left(1,z^2,z^3\right)dz,$$

with $\Delta(k)$ is the domain of integration in the thickness direction of the stiffeners.

The nonlinear compatibility equation for the imperfect panel is derived from Eq. (2) as

$$\hat{\varepsilon}_{x,yy}^0+\hat{\varepsilon}_{y,xx}^0-\hat{\gamma}_{xy,xy}^0=w_{,xy}^2-w_{,xx}/R-w_{,xx}w_{,yy}-w_{,xx}w_{,yy}^*+2w_{,xy}w_{,xy}^*-w_{,xx}^*w_{,yy}. \quad (6)$$

An Airy stress function $\iota(x,y)$ is introduced, satisfying

$$N_x=\iota_{,yy},\qquad N_{xy}=-\iota_{,xy},\qquad N_y=\iota_{,xx}. \quad (7)$$

Using Eqs. (4) and (7), the compatibility equation (6) is reformulated as

$$\begin{aligned}&D_{22}^*\iota_{,xxxx}+\left(D_{66}^*+2D_{12}^*\right)\iota_{,xxyy}+D_{11}^*\iota_{,yyyy}+\left(A_{21}^*-\lambda F_{21}^*\right)\phi_{x,xxx}\\&+\left(\lambda F_{66}^*-\lambda F_{11}^*+A_{11}^*-A_{66}^*\right)\phi_{x,xyy}+\left(\lambda F_{66}^*-\lambda F_{22}^*+A_{22}^*-A_{66}^*\right)\phi_{y,xxy}\\&+\left(A_{12}^*-\lambda F_{12}^*\right)\phi_{y,yyy}-\lambda F_{21}^*w_{,xxxx}-\lambda\left(F_{11}^*+F_{22}^*-2F_{66}^*\right)w_{,xxyy}\\&-\lambda F_{12}^*w_{,yyyy}+w_{,xx}/R-w_{,xy}^2+w_{,xx}w_{,yy}+w_{,xx}w_{,yy}^*-2w_{,xy}w_{,xy}^*+w_{,xx}^*w_{,yy}=0,\end{aligned} \quad (8)$$

In this analysis, FG-GRMMC cylindrical panels are examined under two different boundary conditions.

Case 1: All four edges are simply supported and freely movable (FFFF), leading to

$$\begin{aligned}&N_x=N_{0x}=-hP_x,T_x\big|_{x=0,a}=0,\,M_x\big|_{x=0,a}=0,\,N_{xy}\big|_{x=0,a}=0,\,\phi_y\big|_{x=0,a}=0,\;w\big|_{x=0,a}=0,\\&N_y=N_{0y}=0,T_y\big|_{y=0,b}=0,M_y\big|_{y=0,b}=0,N_{xy}\big|_{y=0,b}=0,\,\phi_x\big|_{y=0,b}=0,\;w\big|_{y=0,b}=0.\end{aligned} \quad (9)$$

Case 2: Two opposite edges $x=0, x=a$ are simply supported and freely movable in x and y directions, while the other two $y=0, y=b$ are simply supported and immovable in y direction (FIFI), with the corresponding conditions

$$\begin{aligned}&N_x=N_{0x}=-hP_x,\;T_x\big|_{x=0,a}=0,\,M_x\big|_{x=0,a}=0,\;N_{xy}\big|_{x=0,a}=0,\,\phi_y\big|_{x=0,a}=0,\;w\big|_{x=0,a}=0,\\&N_y=N_{0y},\;T_y\big|_{y=0,b}=0,\,M_y\big|_{y=0,b}=0,\;v=0,\,\phi_x\big|_{y=0,b}=0,\;w\big|_{y=0,b}=0.\end{aligned} \quad (10)$$

To satisfy the boundary conditions, the deflection, rotation, and initial imperfection shapes are assumed in the form

$$\begin{aligned}&w=W\sin\hat{\alpha}x\sin\hat{\beta}y,\quad w_1=\zeta h\sin\hat{\alpha}x\sin\hat{\beta}y,\\&\phi_x=\Phi_x\cos\hat{\alpha}x\sin\hat{\beta}y,\;\phi_y=\Phi_y\sin\hat{\alpha}x\cos\hat{\beta}y,\end{aligned} \quad (11)$$

where $\hat{\alpha} = m\pi/a, \hat{\beta} = n\pi/b$, m and n are buckling mode numbers in the x and y directions, respectively; W , Φ_x and Φ_y are the corresponding amplitudes of deflection and rotations; and ζ is a dimensionless imperfection parameter.

By substituting Eq. (11) into Eq. (8), the stress function is obtained as

$$\iota = \iota_1 \cos 2\varphi x + \iota_2 \cos 2\eta y + \iota_3 \sin \varphi x \sin \eta y + \frac{1}{2} N_{0y} x^2 + \frac{1}{2} N_{0x} y^2. \tag{12}$$

where

$$\iota_1 = V_{11}\left(W + 2\zeta h\right)W,\ \iota_2 = V_{21}\left(W + 2\zeta h\right)W,\ \iota_3 = V_{31}\Phi_x + V_{32}\Phi_y + V_{33}W,$$

The average sense boundary conditions for immovable edges under FFFF and FIFI conditions are expressed as

$$\begin{aligned} \int_0^b \int_0^a \upsilon_{,y} dxdy &= J_{51}W + J_{52}\Phi_x + J_{53}\Phi_y \\ &+ J_{54}W\left(2\zeta h + W\right) + J_{55}N_{0x} + J_{56}N_{0y} + J_{57}\Delta T = 0, \end{aligned} \tag{13}$$

The total strain energy Γ_{in} of the panel and the potential energy Γ_{ext} due to external loading are evaluated as

$$\Gamma_{in} = \frac{1}{2} \int_{-h/2}^{h/2} \int_0^b \int_0^a \left[\sigma_{xz}\gamma_{xz} + \sigma_y \varepsilon_y + \sigma_{xy}\gamma_{xy} - \alpha(z)\Delta T\left(\sigma_x + \sigma_y\right) + \sigma_{yz}\gamma_{yz} + \sigma_x \varepsilon_x\right] dxdydz, \tag{14}$$

$$\Gamma_{ext} = \int_0^b \int_0^a qw dxdy + N_{0x} \int_0^b \int_0^a u_{,x} dxdy. \tag{15}$$

The Ritz energy method is applied via the total potential energy $\Gamma_{Total} = \Gamma_{in} - \Gamma_{ext}$, as

$$\frac{\partial \Gamma_{Total}}{\partial W} = \frac{\partial \Gamma_{Total}}{\partial \Phi_x} = \frac{\partial \Gamma_{Total}}{\partial \Phi_y} = 0, \tag{16}$$

From Eq. (16), the governing equations are derived in the forms

$$\begin{aligned} &J_{11}W + J_{12}\Phi_x + J_{13}\Phi_y + J_{14}\Phi_x\left(W + \zeta h\right) + J_{15}\Phi_y\left(W + \zeta h\right) + J_{16}W\left(W + 4/3\zeta h\right) \\ &+ J_{17}W\left(W + 2\zeta h\right)\left(W + \zeta h\right) + J_{18}N_{0x} + J_{19}N_{0x}\left(W + \zeta h\right) \\ &+ J_{110}N_{0y} - J_{112}q - J_{113}\Delta T = 0, \end{aligned} \tag{17}$$

$$J_{12}W + J_{22}\Phi_x + J_{23}\Phi_y + J_{24}W\left(W + 2\zeta h\right) + J_{25}N_{0x} + J_{26}N_{0y} - J_{27}\Delta T = 0, \tag{18}$$

$$J_{13}W + J_{23}\Phi_x + J_{33}\Phi_y + J_{34}W\left(W + 2\zeta h\right) + J_{35}N_{0x} + J_{36}N_{0y} - J_{37}\Delta T = 0, \tag{19}$$

Eqs. (17)-(19) are applicable to both boundary conditions. For FFFF, $N_{0x} = -P_x h$ and $N_{0y} = 0$ are used for the FIFI case $N_{0x} = -P_x h$ is applied. Solving Φ_x, Φ_y from Eqs. (18)

and (19) and substituting into Eq. (17) yields. The expression of the axial compression postbuckling curve is obtained in the forms

$$\begin{aligned} P_x = &\Big[\left(\eta_1 e_{11}+\eta_2 e_{21}\right)\hat{W}+\left(\eta_1 e_{12}+\eta_2 e_{22}\right)\Delta T\left(\hat{W}+\zeta\right)+\left(\eta_1 e_{13}+\eta_2 e_{23}\right)\hat{W}h\left(\hat{W}+\zeta\right) \\ &+J_{16}\hat{W}h\left(\hat{W}+\frac{4}{3}\zeta\right)+\left(\eta_1 e_{14}+\eta_2 e_{24}\right)\hat{W}h\left(\hat{W}+2\zeta\right)+\frac{\eta_1 e_{110}\Delta T}{h}+\frac{\eta_2 e_{28}\Delta T}{h}-\frac{J_{112}q}{h} \\ &+\left(\eta_1 e_{15}+\eta_2 e_{25}\right)\hat{W}h^2\left(\hat{W}+2\zeta\right)\left(\hat{W}+\zeta\right)\Big]\Big/\Big[\left(\eta_1 e_{16}+\eta_2 e_{26}\right)+\left(\eta_1 e_{17}+\eta_2 e_{27}\right)h\left(\hat{W}+\zeta\right)\Big], \end{aligned} \tag{20}$$

Similarly, the expression of the external postbuckling curve is

$$\begin{aligned} q = &\Big[\left(\eta_1 e_{11}+\eta_2 e_{21}\right)\hat{W}+\left(\eta_1 e_{12}+\eta_2 e_{22}\right)\Delta T\left(\hat{W}+\zeta\right)+\left(\eta_1 e_{13}+\eta_2 e_{23}\right)\hat{W}h\left(\hat{W}+\zeta\right) \\ &+J_{16}\hat{W}h\left(\hat{W}+\frac{4}{3}\zeta\right)+\left(\eta_1 e_{14}+\eta_2 e_{24}\right)\hat{W}h\left(\hat{W}+2\zeta\right)-\left(\eta_1 e_{16}+\eta_2 e_{26}\right)P_x \\ &-\left(\eta_1 e_{17}+\eta_2 e_{27}\right)P_x h\left(\hat{W}+\zeta\right)+\left(\eta_1 e_{15}+\eta_2 e_{25}\right)\hat{W}h^2\left(\hat{W}+2\zeta\right)\left(\hat{W}+\zeta\right) \\ &+\frac{\eta_1 e_{110}\Delta T}{h}+\frac{\eta_2 e_{28}\Delta T}{h}\Big]\frac{h}{J_{112}} \end{aligned} \tag{21}$$

In the case of a perfect panel without stiffener with $\mu_1 = 0, \mu_2 = 0$ and $\zeta = 0$, the critical buckling load P_x^{cr} is received by applying $\hat{W} \to 0$ as

$$P_x^{cr} = \frac{e_{11}+e_{12}\Delta T}{e_{17}h} \tag{22}$$

3. INVESTIGATION RESULTS AND DISCUSSIONS

Table 1. Comparisons of critical buckling loads $\bar{P}_x^{cr} = P_x^{cr}bh$ (kN) of unstiffened FG-GRMMC laminated cylindrical panels $((0)_{10}$, h =3mm, $a/h = 20$, $b/a = 0.8$, $a/R = 0.8$, m =1, n =1).

T (K)	References	UD	FG-X	FG-O
300	Shen and Xiang [15]	709.81	775.33	654.51
	Present	711.13	774.71	654.17
500	Shen and Xiang [15]	673.93	749.57	619.15
	Present	672.73	725.82	613.18
700	Shen and Xiang [15]	635.97	696.24	580.35
	Present	633.64	693.92	578.22

Table 1 presents a comparison of the critical buckling loads for unstiffened FG-GRMMC cylindrical panels between the present study and the results reported by Shen and Xiang [15], under various thermal environments. In Ref. [15], the authors applied HSDT combined with von Kármán geometric nonlinearity and the singular perturbation technique to obtain analytical solutions for thermomechanical postbuckling behavior. These results validate the accuracy of the formulas established in the present study.

Table 2 examines the effect of temperature on the critical buckling load of unstiffened FG-GRMMC cylindrical panels with different graphene distribution patterns and the GRC

direction arrangements. The results demonstrate that the critical loads of x- and y-stiffened cylindrical panels are approximately equal. These loads decrease as the temperature increases. In addition, among the three investigated material distribution types, the critical buckling loads of the FG-X type are the largest, and those of the FG-O type are the smallest.

Table 2. Critical buckling loads P_x^{cr} (MPa) of unstiffened FG-GRMMC laminated cylindrical panels (h =3mm, $a = b = 20h$, $R = a/0.1$, m =1, n =1).

T (K)	Type	UD	FG-X	FG-O
300	$(0)_{10}$	1779.17	2043.04	1523.47
	$(0/90/0/90/0)_S$	1779.20	2043.06	1523.50
500	$(0)_{10}$	1681.25	1909.58	1427.68
	$(0/90/0/90/0)_S$	1681.28	1909.60	1427.69
700	$(0)_{10}$	1583.99	1834.01	1336.93
	$(0/90/0/90/0)_S$	1584.00	1834.02	1336.95
1000	$(0)_{10}$	1415.06	1620.31	1177.72
	$(0/90/0/90/0)_S$	1415.14	1620.43	1177.79

Figure 2 illustrates the postbuckling responses of FG-GRMMC cylindrical panels with different stiffener types, where the number of stiffeners in each is denoted by n_{st}. It is clear that both orthogonal and oblique stiffeners significantly increase the axial compressive load capacity (Figure 2(a)) and external pressure load capacity (Figure 2(b)) compared to the case of the unstiffened panel. Notably, the postbuckling curves of the stiffened panels with oblique stiffeners are always higher than those of the orthogonally stiffened panels. This improvement is due to the ability of oblique stiffeners to provide multidirectional stiffness and more effective load distribution.

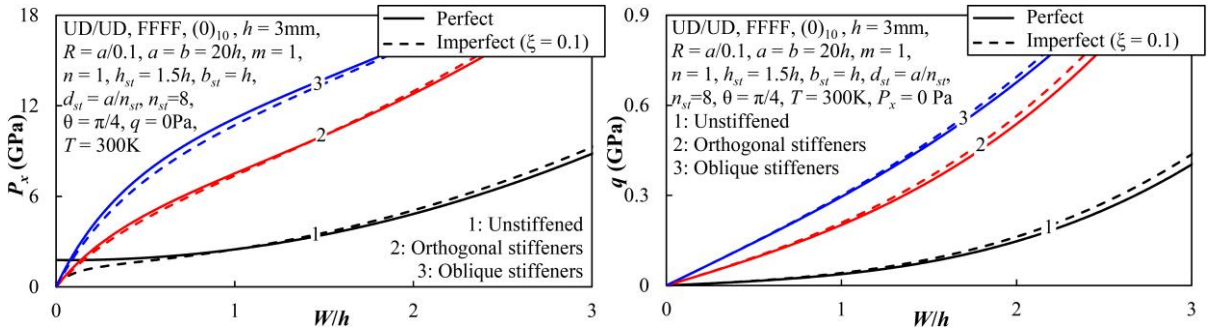

(a) (b)

Figure 2. Effects of stiffener types on the axially compressed and externally pressed postbuckling behavior.

Figure 3 examines the influence of graphene distribution patterns on the postbuckling behavior of the stiffened panel with the oblique stiffeners. Among the considered types, the axially compressed and externally pressed postbuckling curves of the V/A stiffened panel are the highest, and those of the A/V stiffened panels are the lowest. Meanwhile, no significant difference is noted for all three distribution types of X/X, UD/UD, and O/O.

Figure 4 investigates the effect of stiffener angle on the nonlinear postbuckling response of stiffened cylindrical panel. In Figure 4(a), increasing the stiffener angle is proportional to the increase in the axial compressive load capacity of the cylindrical panels. Meanwhile, Figure 4(b) illustrates that under pressure loading, the angle effect of the stiffener is non-

linear and more difficult to predict. The externally pressed postbuckling curve is the highest corresponding to $\theta = \pi / 4$.

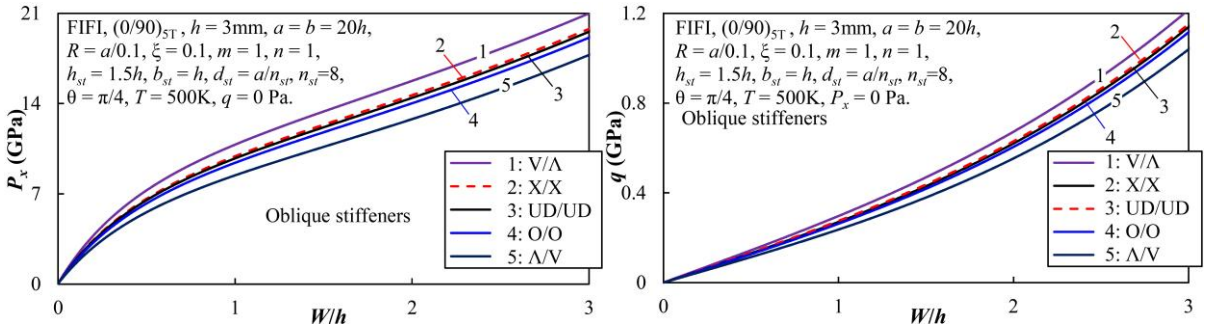

Figure 3. Effects of GRC distribution types on the axially compressed and externally pressed postbuckling behavior.

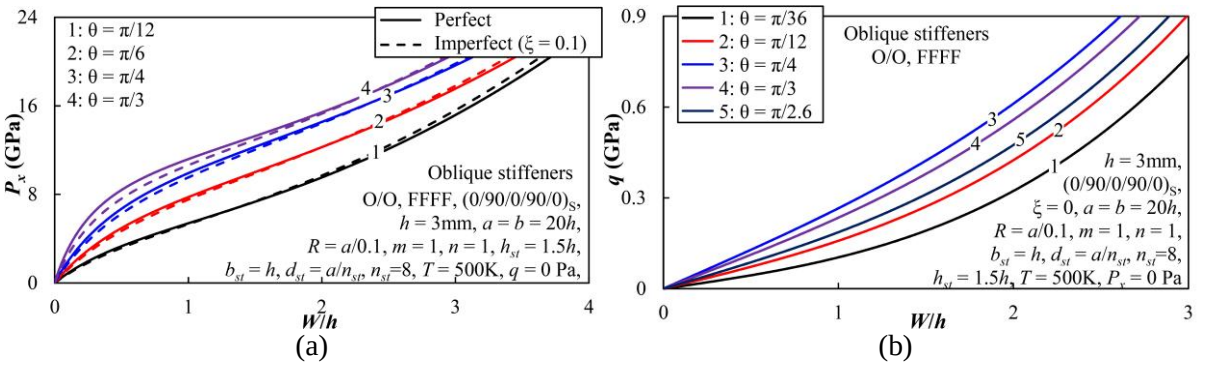

Figure 4. Effects of stiffener angles on the axially compressed and externally pressed postbuckling behavior.

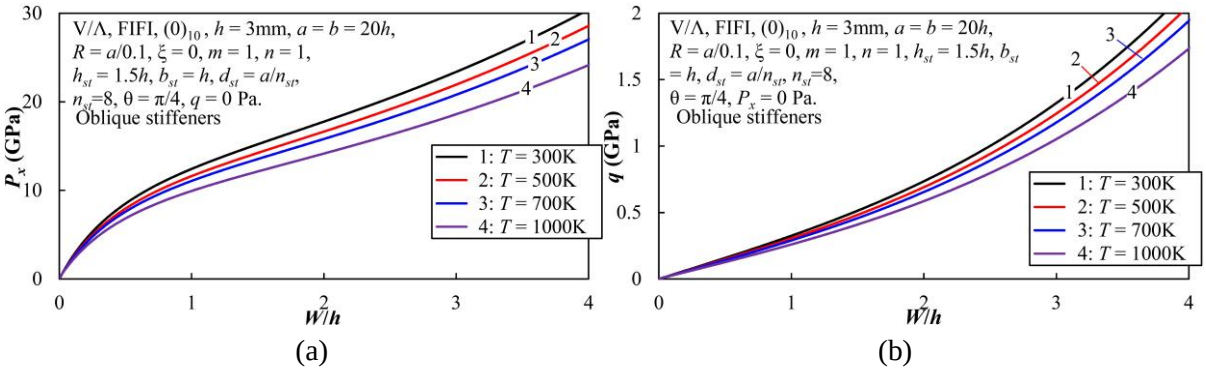

Figure 5. Effects of environment temperatures on the axially compressed and externally pressed postbuckling behavior.

Figure 5 shows the impact of environmental temperature on the mechanical postbuckling curves of a stiffened cylindrical panel. The observed trends are similar to those in Table 2. The axially compressed and externally pressed postbuckling curves are lower as the temperature increases. The cause is the softening of materials due to temperature, particularly with metal matrix. The result is a reduction in the structure's stiffness, which leads to a decreased ability to capacity mechanical loads.

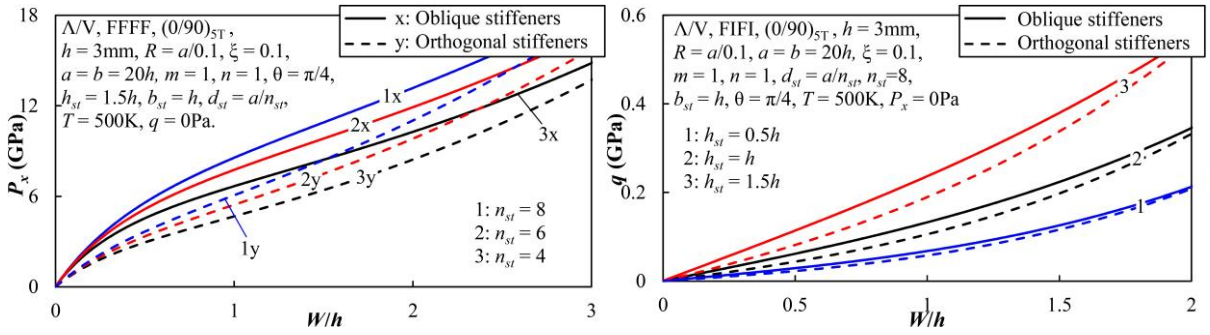

Figure 6. Effects of geometric parameters of stiffeners on the axially compressed and externally pressed postbuckling behavior.

Figure 6 analyzes the effect of stiffener geometry, such as thickness and spacing between stiffeners. Figure 6(a) shows that increasing the number of stiffeners, i.e., increasing the number of stiffeners, will improve the bending resistance after axial loading, because the additional stiffener will improve the local bending stiffness. Figure 6(b) shows that the thickness of the stiffener is proportional to the load-carrying capacity of the stiffened cylindrical panel for both orthogonal and oblique stiffeners.

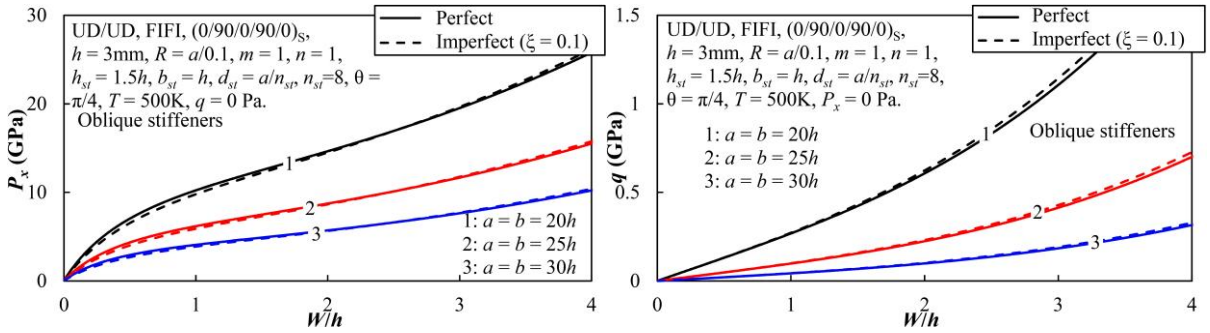

Figure 7. Effects of geometric parameters on the axially compressed and externally pressed postbuckling behavior.

Figure 7 shows the effect of the edge length of the panel on the axial compressive and external pressure load capacity. It is clear that as the length of the edges increases, i.e., the a/h ratio increases, indicating that the panel is thinner, leading to a significant reduction in the mechanical load capacity of the panel. In addition, a faint difference between the mechanical postbuckling curves of the perfect panel and the imperfect panel is also observed in Figures 7(a) and 7 (b).

4. CONCLUSIONS

This study developed an analytical model for the nonlinear buckling and postbuckling problem of FG-GRMMC cylindrical panels stiffened by orthogonal or oblique stiffeners, using HSDT, von Kármán nonlinearity, and the Ritz method. The contribution of stiffeners is modeled by applying an improved smeared stiffener technique with coordinate transformation. Numerical results highlighted several key findings:

1) Oblique stiffeners provide superior postbuckling performance compared to orthogonal ones.

2) The FG-X unstiffened cylindrical panel and the V/A stiffened cylindrical panel have the best load-carrying capacity among the considered material models in the paper.

3) Temperature significantly reduces the axial compressive and external pressure load capacities of stiffened cylindrical panels.

Further studies may consider alternative modeling strategies such as discrete stiffener finite element modeling, equivalent orthotropic layer methods, or artificial intelligence-based optimization frameworks to complement the current analytical approach.

ACKNOWLEDGMENTS

This research is funded by Vietnam National Foundation for Science and Technology Development (NAFOSTED) under grant number 107.02-2023.45.

REFERENCES

[1]. H.S. Shen, H. Wang, Nonlinear bending and postbuckling of FGM cylindrical panels subjected to combined loadings and resting on elastic foundations in thermal environments, Composites Part B: Engineering, 78 (2015) 202–213. https://doi.org/10.1016/j.compositesb.2015.03.078

[2]. H.S. Shen, H. Wang, Thermal postbuckling of FGM cylindrical panels resting on elastic foundations, Aerosp. Sci. Technol., 38 (2014) 9–19. https://doi.org/10.1016/j.ast.2014.07.009

[3]. H. Norouzi, A. Alibeigloo, Three dimensional thermoviscoelastic analysis of a simply supported FGM cylindrical panel, Composite Structures, 148 (2016) 181–190. https://doi.org/10.1016/j.compstruct.2016.03.064

[4]. D. Zhang, D. Li, J. Gao, Z. Wu, C. Jin, On the transient dynamics of FGM cylindrical panels with cutout under thermal shock employing 2D Chebyshev-based energy method, Thin-Walled Struct., 212 (2025) 113176. https://doi.org/10.1016/j.tws.2025.113176

[5]. M. Mirzaei, S. E. Seyedi, Nonlinear vibrations of temperature-dependent FGM cylindrical panels subjected to instantaneous surface heating, Structures, 67 (2024) 106952. https://doi.org/10.1016/j.istruc.2024.106952

[6]. D.H. Bich, D.V. Dung, V.H. Nam, Nonlinear dynamical analysis of eccentrically stiffened functionally graded cylindrical panels, Composite Structures, 94 (2012) 2465–2473. https://doi.org/10.1016/j.compstruct.2012.03.012

[7]. D.T. Dong, V.H. Nam, N.T. Trung, N.T. Phuong, V.T. Hung, Nonlinear thermomechanical buckling of sandwich FGM oblique stiffened plates with nonlinear effect of elastic foundation. Journal of Thermoplastic Composite Materials, 35 (2022) 1441–1467. https://doi.org/10.1177/0892705720935957

[8]. H. Babaei, Thermomechanical analysis of snap-buckling phenomenon in long FG-CNTRC cylindrical panels resting on nonlinear elastic foundation, Composite Structures, 286 (2022) 115199. https://doi.org/10.1016/j.compstruct.2022.115199

[9]. M.M. Keleshteri, H. Asadi, Q. Wang, On the snap-through instability of post-buckled FG-CNTRC rectangular plates with integrated piezoelectric layers, Computer Methods in Applied Mechanics and Engineering, 331 (2018) 53–71. https://doi.org/10.1016/j.cma.2017.11.015

[10]. H.S. Shen, Y. Xiang, Postbuckling of axially compressed nanotube-reinforced composite cylindrical panels resting on elastic foundations in thermal environments, Composites Part B: Engineering, 67 (2014) 50–61. https://doi.org/10.1016/j.compositesb.2014.06.020

[11]. H.S. Shen, Y. Xiang, Thermal postbuckling of nanotube-reinforced composite cylindrical panels resting on elastic foundations, Composite Structures, 123 (2015) 383–392. https://doi.org/10.1016/j.compstruct.2014.12.059

[12]. K. Foroutan, H. Ahmadi, E. Carrera, Nonlinear vibration of imperfect FG-CNTRC cylindrical panels under external pressure in the thermal environment, Composite Structures, 227 (2019) 111310. https://doi.org/10.1016/j.compstruct.2019.111310
[13]. T.Q. Minh, V.M. Duc, D.T. Dong, V.H. Nam, Nonlinear buckling analysis of higher-order shear deformable FG-CNTRC plates stiffened by oblique FG-CNTRC stiffeners, Vietnam J. Mech., 44 (2022) 431–444. https://doi.org/10.15625/0866-7136/17933
[14]. V.M. Duc, T.Q. Minh, N.T. Phuong, V.T. Hung, V.H. Nam, Nonlinear dynamic responses of CNT-reinforced panels with complex curvature, piezoelectric layer, and CNT-reinforced stiffeners, European Journal of Mechanics - A/Solids, 106 (2024) 105341. https://doi.org/10.1016/j.euromechsol.2024.105341
[15]. H.S. Shen, Y. Xiang, Effect of negative Poisson's ratio on the axially compressed postbuckling behavior of FG-GRMMC laminated cylindrical panels on elastic foundations, Thin-Walled Structures, 157 (2020) 107090. https://doi.org/10.1016/j.tws.2020.107090
[16]. H.S. Shen, Y. Xiang, Y. Fan, Postbuckling of functionally graded graphene-reinforced composite laminated cylindrical panels under axial compression in thermal environments, International Journal of Mechanical Sciences, 135 (2018) 398–409. https://doi.org/10.1016/j.ijmecsci.2017.11.031
[17]. H.S. Shen, Y. Xiang, J.N. Reddy, Thermal postbuckling behavior of FG-GRC laminated cylindrical panels with temperature-dependent properties, Composite Structures, 211 (2019) 433–442. https://doi.org/10.1016/j.compstruct.2018.12.023
[18]. N.T. Phuong, D.T. Dong, C.V. Doan, V.H. Nam, Nonlinear buckling of higher-order shear deformable stiffened FG-GRC laminated plates with nonlinear elastic foundation subjected to combined loads, Aerospace Science and Technology, 127 (2022) 107736. https://doi.org/10.1016/j.ast.2022.107736
[19]. Y. Fan, Y. Xiang, H.S. Shen, Temperature-dependent mechanical properties of graphene/Cu nanocomposites with in-plane negative Poisson’s ratios, Research, 2020 (2020) 5618021. https://doi.org/10.34133/2020/5618021